

Iterative coupling of FEM and BEM in 3D transient elastodynamics

Otto von Estorff ^{*}, Christian Hagen ¹

Institute of Modelling and Computation, Hamburg University of Technology, Denickestr. 17, 21073 Hamburg, Germany

Abstract

A domain decomposition approach is presented for the transient analysis of three-dimensional wave propagation problems. The subdomains are modelled using the FEM and/or the BEM, and the coupling of the subdomains is performed in an iterative manner, employing a sequential Neumann–Dirichlet interface relaxation algorithm which also allows for an independent choice of the time step length in each subdomain. The approach has been implemented for general 3D problems. In order to investigate the convergence behaviour of the proposed algorithm, using different combinations of FEM and BEM subdomains, a parametric study is performed with respect to the choice of the relaxation parameters. The validity of the proposed method is shown by means of two numerical examples, indicating the excellent accuracy and applicability of the new formulation.

© 2006 Elsevier Ltd. All rights reserved.

Keywords: Domain decomposition; Iterative coupling; FEM; BEM; 3D elastodynamics; Transient analysis; Different time steps

1. Introduction

In many fields of engineering mechanics, the Finite Element Method (FEM) and the Boundary Element Method (BEM) are valuable and frequently applied analysis tools. Each one of these methods has its specific areas of application. The FEM, for instance, is especially well suited for the analysis of problems involving inhomogeneities or non-linear behaviour of the considered solid bodies [1,2], while the BEM has some advantages if stress singularities or unbounded subregions are present, or- in dynamics-, if incident wave fields need to be considered [3–5].

Therefore, for problems involving subregions with different characteristics, it seems to be a natural approach to combine the FEM and BEM within a single computational model, thus making use of the respective advantages of both methods. This is done by decomposing the considered domain into several subdomains, where each subdomain, according to its specific physics, is modelled either by the FEM or the BEM [6–8]. Then, the subdomains are coupled to each other, taking into account the appropriate compatibility and equilibrium

conditions at the respective interface boundaries. This is called the *domain decomposition* or *subdomain approach*.

Domain decomposition can also be useful within pure BEM models, where no FEM subdomains are considered. Typically, this is needed if regions with different material properties (e.g. layered soils) or even different physics (e.g. in solid–fluid coupling) are to be analysed [9–13]. Furthermore, a pure BEM domain decomposition can also be employed in order to improve the efficiency and the numerical properties of the model [14], or to enable parallel computations [13–15].

Regarding applications in dynamics, a rather complete overview over FEM–BEM and BEM–BEM coupling procedures is given by Beskos [16–18]. Usually, the coupling is performed directly, i.e. the equations for all subdomains are assembled into a single, global, equation system. Direct FEM–BEM coupling in the time–domain is treated, e.g. by Karabalis and Beskos [19], Fukui [20], and von Estorff and Prabucki [21] for linear cases, and by Pavlatos and Beskos [22], Adam [23], Abouseeda and Dakoulas [24], Yazdchi et al. [25], and Firuziaan and von Estorff [26], taking non-linearities in the FEM subdomain into account.

Alternatively, either staggered or iterative methods can be used, where the equations for the subdomains are solved separately. Thus, the assembly and solution of a global, coupled equation system is avoided. Such an approach offers considerable advantages over the direct coupling procedure. First, specialized solvers can be used for solving the system of equations of each subdomain, taking full advantage of the respective matrix characteristics. For example, the FEM system matrix usually is symmetric, while the BEM system

^{*} Corresponding author. Fax: +49 40 42 878 4353.

E-mail addresses: estorff@tu-harburg.de (O. von Estorff), hagen@tu-harburg.de (C. Hagen).

¹ Supported by DFG.

matrix is not. This can be accounted for the choice of the solvers in order to save computational time. Second, the use of different time step lengths for the subdomain is possible. This is an important advantage, especially in the BEM, where the range of applicable time step lengths, resulting in a stable and accurate solution, is limited. Finally, the numerical characteristics of a global coupled system matrix are often very bad when compared to the characteristics of the separate subdomain matrices. The general disadvantage of being an approximative method is not really an issue, since, the approximation error becomes much smaller than the discretization error, if appropriate convergence measures are employed.

In the *staggered solution approach*, which can be applied to transient dynamic analyses only, the equations for each subdomain are solved once at each time step, and predicted values of the coupling boundary conditions are used. Hence, the suitable choice of the predictor operator, which also depends on the selected time integration scheme, as well as the use of sufficiently small time steps, is crucial for the accuracy of this procedure. The approach is described in detail by Park and Felippa [27] for a variety of coupled dynamic problems in mechanics. These authors also consider the inclusion of a corrective iteration at each time step, but find that reducing the time step size is more effective than an iterative solution for the class of problems they are interested in, namely the coupling of first-order and second-order algebraic equation systems.

Rizos and Wang [28] have developed a staggered FEM–BEM coupling approach for the time–domain analysis of wave propagation problems that furthermore allows for the selection of different time step lengths in the subdomains. They use a BEM that is based on B-Spline fundamental solutions, and report good accuracy for several examples involving soil–structure interaction.

However, staggered approaches should be used with great care only, since their characteristics regarding stability and accuracy of the solution is often not satisfactory [29]. Furthermore, the stability and accuracy of both the BEM itself and the staggered coupling approach impose requirements on the choice of the time step durations, which may be contradictory. Therefore, it is desirable to use a coupling procedure that is stable and accurate for a wide range of time step durations. This can be obtained by introducing corrective iterations into the staggered algorithm [29,30].

If a corrective iteration at each time step is employed, where the interface boundary conditions are iteratively updated until convergence is achieved, one obtains an *iterative coupling method*. Within the iteration procedure, a relaxation operator may be applied to the interface boundary conditions in order to enable or speed up convergence. In this case, the method can also be called an *interface relaxation method*. An overview over a variety of such techniques for static analyses, involving FEM–BEM as well as BEM–BEM coupling, is given by El-Gebeily et al. [31] and Elleithy and Tanaka [32]. These authors also report a number of applications to potential flow as well as elastostatic problems.

An interface relaxation algorithm for the iterative coupling of one FEM and BEM domain was developed by Lin et al. [33]

and Feng and Owen [34] for application in two-dimensional linear elastostatics. In that method, initially the displacements at the interface are guessed and assigned to the BEM subdomain as boundary conditions. The corresponding interface forces are then determined from the BEM system of equations and directly assigned to the FEM subdomain. Thereafter, the FEM equation system is solved to obtain a new guess of the interface displacements. Relaxed values of the displacements are assigned to the BEM subdomain in turn, starting the next iteration step, until convergence is achieved. This algorithm was investigated in detail with respect to its convergence characteristics by Elleithy and co-workers [31,35]. It was found that the convergence of the algorithm depends on a large number of influence factors, such as the geometrical and material properties of the subdomains, the specified types of the boundary conditions, the mesh density, and, most important, on the relaxation parameter inherent to the proposed algorithm.

The same algorithm was modified by Soares et al. [30] and extended for application to 2D transient electrodynamics problems, where different time step lengths in the two subdomains can be employed. Furthermore, possible nonlinearities in the FEM subdomain are taken into account, and the coupling iterations are performed very effectively together with the FEM equilibrium iterations. Thus, in non-linear transient analysis, the extra computational costs of the corrective iterations—as compared to the staggered approach without iterations—are very low, while the accuracy of the solution is highly improved.

The original algorithm [33,34] may be considered as a sequential Dirichlet–Neumann method with single relaxation, while the modified method [30] may be considered as a sequential Neumann–Dirichlet method with single relaxation. The present paper deals with the extension of the latter, such that an investigation of arbitrary 3D systems and BEM–BEM as well as FEM–FEM coupling becomes also possible. For this purpose, a second relaxation step is introduced. Hence, the new algorithm may be called a sequential Neumann–Dirichlet method with double relaxation. The new method is applied to some illustrative problems in 3D transient elastodynamics. A parametric study investigates the suitable choice of the relaxation parameters, as well as the influence of the combination of the analysis methods used for the subdomains, and of the time step ratios.

In Section 2 of this paper, the formulation of the non-linear transient elastodynamic FEM is outlined. Section 3 introduces the transient elastodynamic BEM formulation which is used here. Details about the proposed coupling algorithm are given in Section 4. A parametric study is described in Section 5, while Section 6 introduces the numerical examples to show the accuracy of the proposed methodology.

2. Finite element method

Employing the displacement-based finite element method, the dynamic equilibrium equations for a general solid body at a given time t can be written as [1]

$$M^t \ddot{u} + {}^t K^t u = {}^t f, \tag{1}$$

where the upper left index t marks quantities at the current time: ${}^t u$ is the vector of nodal displacements, ${}^t \ddot{u}$ is the vector of nodal accelerations, and M is the time-independent mass matrix. The matrix ${}^t K = {}^t K({}^t u)$ denotes the stiffness matrix, which may depend on the current deformation state ${}^t u$ as well as on the deformation history, and ${}^t f$ is the vector of external nodal forces.

The considered time period is divided into a number of time steps, each having the duration Δt , and an implicit time integration scheme, such as Newmark’s method, is applied. Taking possible non-linearities of the stiffness matrix ${}^t K$ into account, an incremental solution procedure is employed, where at each time step an equilibrium iteration is performed.

Thus, in each iterative step an equation of the form

$${}^{t-\Delta t} \hat{K} \Delta_k u = {}^t f + {}_{k-1} r \tag{2}$$

has to be solved, where the lower left index k marks quantities at the current iteration step, $\Delta_k u$ is the vector of nodal displacement increments, contributing to the total nodal displacements such that

$${}_k u = {}_{k-1} u + \Delta_k u \tag{3}$$

while ${}^{t-\Delta t} \hat{K}$ is the effective tangent stiffness matrix, which contains also influences from inertial effects, ${}^t f$ is the vector of applied nodal forces, and ${}_{k-1} r$ is a vector that comprises influences from inertial forces and from internal element stresses corresponding to the previous step of the iteration.

3. Boundary element method

Consider an arbitrary solid body, consisting of an homogeneous, isotropic, linearly elastic material and subjected to boundary conditions which are given as transient traction loads or imposed displacements at the surface of the body or as an incident displacement wave field. The surface is discretized by means of elements, which are connected by their nodes, and the boundary conditions are selected in such a way that all displacements remain small compared to the dimensions of the body. Moreover, a time period, divided into a finite number of time steps, each having the duration Δt , shall be considered, and it is assumed that the body under investigation is initially at rest.

The time-domain boundary element method then yields an algebraic equation of the form [4,5,36]

$${}^1 T^t u = {}^1 U^t t + \sum_{k=1}^{m-1} ({}^{m-k+1} \Delta t) U^k \Delta t t - ({}^{m-k+1} \Delta t) T^k \Delta t u + {}^t u^{inc} \tag{4}$$

which is valid at any time step m , referring to the time instance $t = m\Delta t$, and relates the nodal values of the surface tractions to those of the displacements. In Eq. (4), ${}^\tau T$ and ${}^\tau U$ are the so-called influence matrices for the retarded time τ , ${}^\tau u$ and ${}^\tau t$ are the vectors of nodal displacements and tractions at time τ , and ${}^t u^{inc}$ are displacements referring to an incident wave field,

e.g. caused by an earthquake. The sum on the right hand side represents the (known) influence of all previous time steps.

In order to use concentrated nodal forces instead of surface tractions, it is necessary to transform the fractions in Eq. (4) into nodal forces. Therefore, a transformation matrix A is introduced, which facilitates the computation of energetically equivalent nodal forces from given tractions [13], and which therefore is defined by ${}^t f = A^t t$, with ${}^t f$ being the vector of nodal forces.

Introducing this transformation matrix into Eq. (4) yields

$${}^1 T^t u = {}^1 \check{U}^t f + {}^t h, \tag{5}$$

where the matrix ${}^1 \check{U}$ is given by ${}^1 \check{U} = {}^1 U A^{-1}$. Furthermore, the sum term and the term representing the influence wave field in Eq. (4) have been replaced by the abbreviation ${}^t h$.

Before Eq. (5) can be solved, the matrices and vectors have to be re-arranged, yielding

$$Y^t x = X^t y + {}^t h, \tag{6}$$

where vector ${}^t x$ contains the *unknown* nodal forces and displacement values at the current time step, while in ${}^t y$ the according *known* values are assembled. Note that the matrices X and Y are constant for all time steps. Eq. (6) is solved time step by time step, starting from $t = \Delta t$ and continuing in a time-marching manner.

4. Iterative coupling of two subdomains

4.1. Domain decomposition

Consider an arbitrary 3D solid body Ω , which is decomposed arbitrarily into two subdomains Ω_1 and Ω_2 . Each subdomain can be treated using either the FEM or the BEM, i.e. the Eqs. (2) and (6) are used, respectively. It is required that the locations of the nodal points of both subdomains match along the interface.

The coupling of the subdomains is ensured by imposing the appropriate compatibility and equilibrium conditions at the interface boundaries. In the proposed method, these conditions are formulated as compatibility of the displacements and equilibrium of the forces at the interface nodes, i.e.

$$u_{1,c} = u_{2,c} \tag{7}$$

and

$$f_{1,c} + f_{2,c} = 0, \tag{8}$$

where the subscripts $1,c$ and $2,c$ mark the coupled nodal degrees of freedom in Ω_1 and Ω_2 , respectively.

For each subdomain, the time step duration may be chosen arbitrarily. Thus, the time step durations for all subdomains can be adjusted according to stability and accuracy considerations, which in turn depend on the applied analysis method and the material parameters. The shorter one of the two time steps is labelled as the *reference* time step

$$\Delta t_{ref} = \min(\Delta t_1, \Delta t_2), \tag{9}$$

where the time step durations associated with Ω_1 and Ω_2 are denoted by Δt_1 and Δt_2 , respectively. The domain, for which the reference (i.e. shorter) time step duration is defined, is called *reference domain* hereafter, and its associated quantities are marked by the subscript ‘ref’, while quantities associated to the other, non-*reference*, domain are marked by the subscript ‘long’, such as

$$\Delta t_{\text{long}} = \max(\Delta t_1, \Delta t_2). \tag{10}$$

4.2. Iterative coupling algorithm

The proposed algorithm is based on the sequential Neumann–Dirichlet method with single relaxation, which has been developed by Soares et al. [30] for 2D investigations. In the present work, however, a second relaxation pass is introduced in order to improve the convergence behaviour. Thus, a sequential Neumann–Dirichlet method with double relaxation is obtained. Moreover, the model has been extended to the investigation of 3D problems.

As outlined previously, the computations for each subdomain are performed separately, and the coupling of the subdomains, i.e. the satisfaction of the coupling conditions (7) and (8), is enforced at a number of discrete time instances, namely at each reference time step

$${}^m t_{\text{ref}} = m \Delta t_{\text{ref}}, \quad m = 1, 2, 3, \dots \tag{11}$$

Due to the possibility that the durations of the time steps are different, the two subdomain equations generally cannot be solved for the same instance of time. Instead, the equations are solved for different times ${}^m t_{\text{ref}}$ (reference domain) and ${}^p t_{\text{long}} = p \Delta t_{\text{long}}$, $p = 1, 2, 3, \dots$ (non-reference domain), and the values from the non-reference domain are interpolated or extrapolated in order to obtain the values at the time instance ${}^m t_{\text{ref}}$, at which the coupling is performed. Correspondingly, extrapolation or interpolation is employed to obtain the values at the non-reference time ${}^p t_{\text{long}}$ from those at the reference time, where necessary.

In the time-domain BEM scheme, which was outlined in Section 3, the surface tractions or nodal forces usually are assumed to remain constant within each time step, while the displacements are assumed to vary linearly with time. Therefore, in the case of BEM nodal forces, *constant* time

interpolation or extrapolation is employed, while in all other cases *linear* interpolation or extrapolation is used.

At any reference step m , the non-reference step number p is chosen such that

$${}^m t_{\text{ref}} - \vartheta \Delta t_{\text{long}} \leq {}^p t_{\text{long}} < {}^m t_{\text{ref}} + (1 - \vartheta) \Delta t_{\text{long}}, \tag{12}$$

where $\vartheta \geq 0$ is a parameter which controls the update of the time ${}^p t_{\text{long}}$ in order to avoid extreme extrapolations. This means, if $\vartheta = 0$, always ${}^p t_{\text{long}} \geq {}^m t_{\text{ref}}$ holds. If $\vartheta > 0$, however, in cases when otherwise ${}^{p-1} t_{\text{long}}$ would be only slightly smaller than ${}^m t_{\text{ref}}$, the update of the non-reference time is delayed and ${}^p t_{\text{long}} < {}^m t_{\text{ref}}$ is enforced.

The effect of ϑ on the determination of the coupling forces at the time t_1 —in the case that the reference domain is Ω_2 —is shown in Fig. 1. Accordingly, the effect on the determination of the coupling displacements at t_2 in the case that the reference domain is Ω_1 is similar. The authors found a choice of $\vartheta \approx 0.2$ to be generally suitable.

Further details on the proposed algorithm are given in Table 1.

The formulation includes two independent relaxation operations (steps 2.4.4 and 2.4.9 in Table 1), controlled by the parameters ω_u and ω_f . In order to obtain some information about how to choose these parameters, a parametric study has been performed (see Section 5).

4.3. Convergence criteria

When using iterative solution procedures, the appropriate identification of convergence is essential. In the present study, four different convergence criteria are employed, which will be outlined in the following.

The first of the convergence criteria is based on a displacement increment measure and is given by

$$\frac{\| {}_k^{t_{\text{ref}}} \mathbf{u}_{1,c}^* - {}_{k-1}^{t_{\text{ref}}} \mathbf{u}_{2,c} \|_2}{\| {}_k^{t_{\text{ref}}} \mathbf{u}_{2,c} \|_2} < \varepsilon_u \tag{13}$$

The second criterion is based on an unbalanced forces measure:

$$\frac{\| {}_k^{t_{\text{ref}}} \mathbf{f}_{2,c}^* + {}_{k-1}^{t_{\text{ref}}} \mathbf{f}_{1,c} \|_2}{\| {}_k^{t_{\text{ref}}} \mathbf{f}_{1,c} \|_2} < \varepsilon_f \tag{14}$$

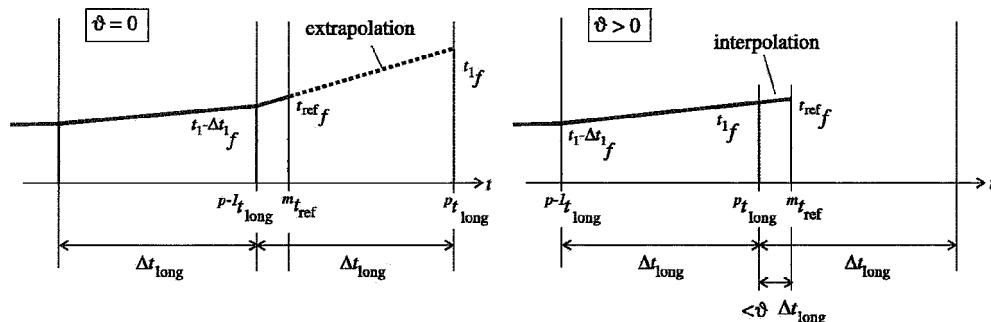


Fig. 1. Effect of the parameter ϑ on the determination of the coupling forces ${}^l f_c$ at time $t_1 = {}^p t_{\text{long}}$ in the case that the reference domain is Ω_2 .

Table 1

Algorithm for the iterative coupling

-
1. *Initial settings.* Set $t_1=0, t_2=0$ and $\Delta t_{\text{ref}}=\min(\Delta t_1, \Delta t_2)$ (note that either $t_1 \equiv t_{\text{ref}}, t_2 \equiv t_{\text{long}}$ or $t_1 \equiv t_{\text{long}}, t_2 \equiv t_{\text{ref}}$)
 2. *Time loop* over all reference time steps
 - 2.1 Update reference time: $t_{\text{ref}} \rightarrow t_{\text{ref}} + \Delta t_{\text{ref}}$
 - If $t_{\text{ref}} > t_{\text{stop}}$, finish the analysis
 - If $t_{\text{long}} < t_{\text{ref}} - \vartheta \Delta t_{\text{long}}$ update non-ref. time: $t_{\text{long}} \rightarrow t_{\text{long}} + \Delta t_{\text{long}}$
 - 2.2. Update time ratio parameter: $\lambda = (t_{\text{long}} - t_{\text{ref}}) / \Delta t_{\text{long}}$
 - 2.3. Set iteration counter $k=0$. Choose initial coupling forces $f_{1,c}^{t_{\text{ref}}}$
 - 2.4 *Iterative loop* until convergence
 - 2.4.1 If $t_1 \neq t_{\text{ref}}$, perform time extrapolation of coupling forces in order to obtain forces at time t_1

$$f_{1,c}^{t_1} = \begin{cases} f_{1,c}^{t_{\text{ref}}} & \text{if } \Omega_1 \text{ is a BEM domain} \\ (1-\lambda)^{-1} (f_{1,c}^{t_{\text{ref}}} - \lambda^{t_1 - \Delta t_1} f_{1,c}^{t_{\text{ref}}}) & \text{if } \Omega_1 \text{ is a FEM domain} \end{cases}$$
 - 2.4.2 Apply $f_{1,c}^{t_1}$ as boundary conditions to Ω_1 , and solve system of Eqs. (2) or (6), respectively, for this domain (at time t_1). Displacements $u_{1,c}^{t_1}$ are obtained
 - 2.4.3 If $t_1 \neq t_{\text{ref}}$, time interpolation of displacements to obtain displacements at time t_{ref} : $u_{1,c}^{t_{\text{ref}}} = (1-\lambda)_k^t u_{1,c}^* + \lambda^{t_1 - \Delta t_1} u_{1,c}$
 - 2.4.4 Perform relaxation of the displacements: $u_{2,c}^{t_{\text{ref}}} = \omega_{uk} u_{1,c}^* + (1-\omega_{uk}) u_{2,c}^{t_{\text{ref}}}$
 - 2.4.5 If $t_2 \neq t_{\text{ref}}$, perform time extrapolation of displacements to obtain displacements at time t_2 : $u_{2,c}^{t_2} = (1-\lambda)^{-1} (u_{2,c}^{t_{\text{ref}}} - \lambda^{t_2 - \Delta t_2} u_{2,c}^{t_{\text{ref}}})$
 - 2.4.6 Apply $u_{2,c}^{t_2}$ as boundary conditions to Ω_2 , and solve system of Eqs. (2) or (6), respectively, for this domain (at time t_2) Coupling forces $f_{2,c}^{t_2}$ are obtained
 - 2.4.7 If $t_2 \neq t_{\text{ref}}$, perform time interpolation of coupling forces in order to obtain forces at time t_{ref} : $f_{2,c}^{t_{\text{ref}}} = \begin{cases} f_{2,c}^{t_2} & \text{if } \Omega_1 \text{ is a BEM domain} \\ (1-\lambda)_k^t f_{2,c}^* + \lambda^{t_2 - \Delta t_2} f_{2,c} & \text{if } \Omega_1 \text{ is a FEM domain} \end{cases}$
 - 2.4.8 Check for convergence If convergence is achieved, jump back to 2.1 and start next time step
 - 2.4.9 Perform relaxation of the coupling forces in order to obtain the new coupling forces for Ω_1 : $f_{1,c}^{t_{\text{ref}}+1} = -\omega_{fk} f_{2,c}^* + (1-\omega_{fk}) f_{1,c}^{t_{\text{ref}}}$
 - 2.4.10 Update iteration counter $k \rightarrow k+1$. Go back to 2.4.1
 - 3 End of analysis
-

Note that due to (8) the coupling forces at Ω_1 are reversed when compared to those at Ω_2 .

When domain decomposition is used, the coupling interfaces may be located at some distance from the zones, where loads are applied. Therefore, in wave propagation problems, it may take several time steps for the waves to reach a coupling interface. During that time period, i.e. before any wave has reached the interface, the interface itself remains in tranquillity. Consequently, the exact solution for the coupling forces as well as for the displacements at the coupling interface is zero. In such cases, both of the aforementioned convergence measures are not appropriate, since they employ a division by zero (or by a quantity which is very close to zero).

Therefore, two additional convergence measures are introduced, which compare the displacement increments and the unbalanced forces at the coupling interface to the *prescribed* displacements and forces, respectively, at other parts of the boundaries. The first of these criteria is

$$\frac{\|f_{1,c}^{t_{\text{ref}}} - f_{1,c}^{t_{\text{ref}}-1}\|_2}{\|f_p^{t_{\text{ref}}}\|} < \varepsilon_v \quad (15)$$

where

$$\|f_p^{t_{\text{ref}}}\| = \sum_{\kappa=1}^2 \left(\sqrt{\frac{n_{\text{dof},c}^\kappa}{n_{\text{dof}}^\kappa}} \|f_{k,p}^{t_{\text{ref}}}\|_2 \right) \quad (16)$$

is a weighted norm of the prescribed displacements at the subdomains, where n_{dof}^κ and $n_{\text{dof},c}^\kappa$ are the total number of degrees of freedom and the number of coupled degrees of freedom, respectively, of the domain no. κ . The vector $f_{k,p}^{t_{\text{ref}}}$

contains the prescribed nodal displacements in the domain no. κ at the current time.

A second, similar criterion can be constructed for the coupling forces. One obtains

$$\frac{\|f_{2,c}^{t_{\text{ref}}} - f_{2,c}^{t_{\text{ref}}-1}\|_2}{\|f_p^{t_{\text{ref}}}\|} < \varepsilon_g \quad (17)$$

where

$$\|f_p^{t_{\text{ref}}}\| = \sum_{\kappa=1}^2 \left(\sqrt{\frac{n_{\text{dof},c}^\kappa}{n_{\text{dof}}^\kappa}} \|f_{k,p}^{t_{\text{ref}}}\|_2 \right) \quad (18)$$

is a norm of the prescribed nodal forces, and $f_{k,p}^{t_{\text{ref}}}$ is a vector that contains the prescribed nodal forces in the domain no. κ .

Convergence is assumed to be achieved either if criteria (13) and (14) are satisfied, or if criteria (15) or (17) is satisfied.

With respect to the fact that in the cases when the criteria (15) or (17) are to be applied, the exact solution is zero, i.e. much smaller than the applied forces or displacements, the tolerances ε_v and ε_g should be chosen considerably smaller than ε_u and ε_f . In this way, it is also guaranteed that the latter convergence criteria do not spoil the accuracy of the results in those time steps, where the interface is no longer in tranquillity.

In all the examples presented hereafter, the convergence tolerances $\varepsilon_u = \varepsilon_f = 1.0 \times 10^{-3}$ and $\varepsilon_v = \varepsilon_g = 1.0 \times 10^{-5}$ are chosen.

5. Parametric study

The convergence characteristics of the sequential Dirichlet–Neumann FEM–BEM iterative coupling method was studied

extensively by Elleithy and co-workers [31,35]. Interestingly, these researchers found that the initial guess of the interface displacement does not influence the existence of convergence. (It only has a slight effect on the rate of convergence, though.) Whereas, the convergence does depend on the mesh density of the subdomains, the specified types of boundary conditions, and the geometrical as well as material properties. Most importantly, it depends on the selection of the relaxation parameter.

It seems natural that these findings can be transferred to the time-domain algorithm proposed in the present paper. Moreover, the choice of the analysis methods for the subdomains, as well as the choice of the respective time step durations, may also influence the convergence behaviour. In order to obtain some information about these factors and to provide some guidelines on the selection of the relaxation parameters ω_f and ω_u , parametric study has been performed.

An elastic rod (length 12 m, cross-section 6 m \times 6 m), consisting of an homogeneous, linearly elastic material with Young's modulus $E=1.0 \times 10^6$ kN/m², Poisson's ratio $\nu=0.25$, and mass density $\rho=1.0$ t/m³ (P-wave velocity $c_1=1095.5$ m/s), is analyzed. The rod is fixed at one end, and excited by a surface traction at the other, free end, while the remaining surfaces are fraction free (Fig. 2 left). The excitation varies in time in the form of a sine function with a period of $T=0.025$ s.

The computational model is decomposed into two subdomains, each having the dimensions 6 m \times 6 m \times 6 m and being modelled using either the FEM or the BEM (Fig. 2 tight). Elements with quadratic shape functions are used (FEM: 20-node solid elements BEM: 8-node surface elements). The length of all element edges is 2 m.

For the two subdomains, four different combinations of analysis methods are considered: (I) BEM–BEM, (II) FEM–FEM, (III) FEM–BEM and (IV) BEM–FEM. In the two latter cases, the BEM domain is the *upper* part of the rod, i.e. that part, where the load is applied, while the FEM domain is the lower part with the fixed end. The difference between the models is, that in Model (III), Ω_1 is the *FEM* subdomain, while in Model (IV), Ω_1 is the *BEM* subdomain (adopting the

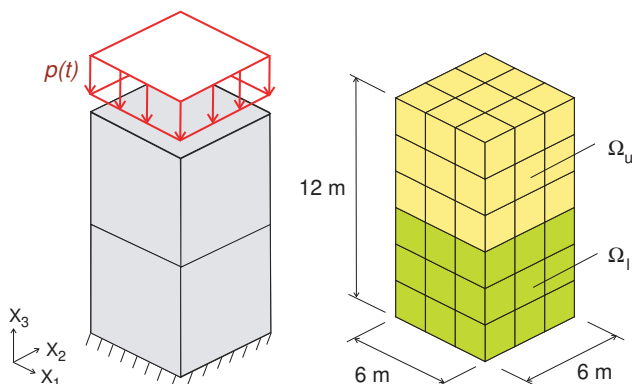


Fig. 2. Elastic rod model for the parametric study: boundary conditions (left) and discretization (right).

notation from Section 4 and from the algorithm given in Table 1).

The time step duration Δt for the calculations is chosen to be optimal with respect to stability and accuracy of the BEM. Therefore, it mainly depends on the spatial discretization and on the wave propagation velocities in the material. Frequently, the dimensionless parameter β is employed, which is given by

$$\beta = \frac{c\Delta t}{l_\beta}, \quad (19)$$

where c is the wave propagation velocity corresponding to the predominant wave form (P- or S-wave) in the problem, and l_β is a discretization parameter, which may be chosen as the mean value of the distances between neighbouring nodes.

In the time-domain BEM, the value of β is restricted to a very small range, where stable and satisfactory results are achieved. This range is frequently reported to be about $0.7 < \beta < 1.2$ for 3D elastodynamics [5,37,38].

In the present case, the value $\beta=1.0$ is used, and the predominant wave form is the P-wave with $c=c_1=1095.5$ m/s. Owing to the homogeneity of the mesh, l_β is easily determined to be 1.0 m in the present case. Thus, from Eq. (19) one obtains an optimal time step duration of $\Delta t_{BE}=0.91 \times 10^{-3}$ s for the BEM subregion.

In the parametric studies, equal time step durations $\Delta t_{FE}=\Delta t_{BE}$ for both subdomains are employed. Additionally, Model (III) is analysed using different time step ratios $\Delta t_{FE}/\Delta t_{BE}=1.5$ (Model IIIb), 0.7 (IIIc), 0.5 (IIId) and 0.3 (IIIe).

With each one of the abovementioned models, parametric studies are performed with respect to the relaxation parameters ω_u and ω_f . Each of the parameters is varied in the range from 0.2 to 1.0 in steps of 0.05. The considered problem then is solved for 20 time steps, and the average number of iterations per time step is determined. If after 30 iterations, no convergence could be achieved, the calculation is stopped.

The results of the parametric studies are shown in Figs. 3 and 4. It can be seen that the convergence characteristics are very different, depending on the subdomain analysis methods as well as on the time step ratios.

The further (dependence on the subdomain analysis methods) is in accordance with the findings of Elleithy and Tanaka [39], who formally analysed the convergence behaviour of the Dirichlet–Neumann FEM–BEM coupling algorithm (with single relaxation), where the Dirichlet interface boundary data is applied to the FEM domain, and compared it to the behaviour of the same algorithm, where the Dirichlet data is applied to the *BEM* domain instead [31].

They found that the conditions of convergence, in particular the choice of the relaxation parameter, are formally different in the two variants of the method. A parametric study confirms the formal findings.

As one can see from the results given in Fig. 3, the same seems to be true for the four variants of the Neumann–Dirichlet subdomain coupling algorithm analysed in the present paper. Moreover, the dependence on the two relaxation parameters is nearly symmetric in all cases analysed here. Therefore, in these

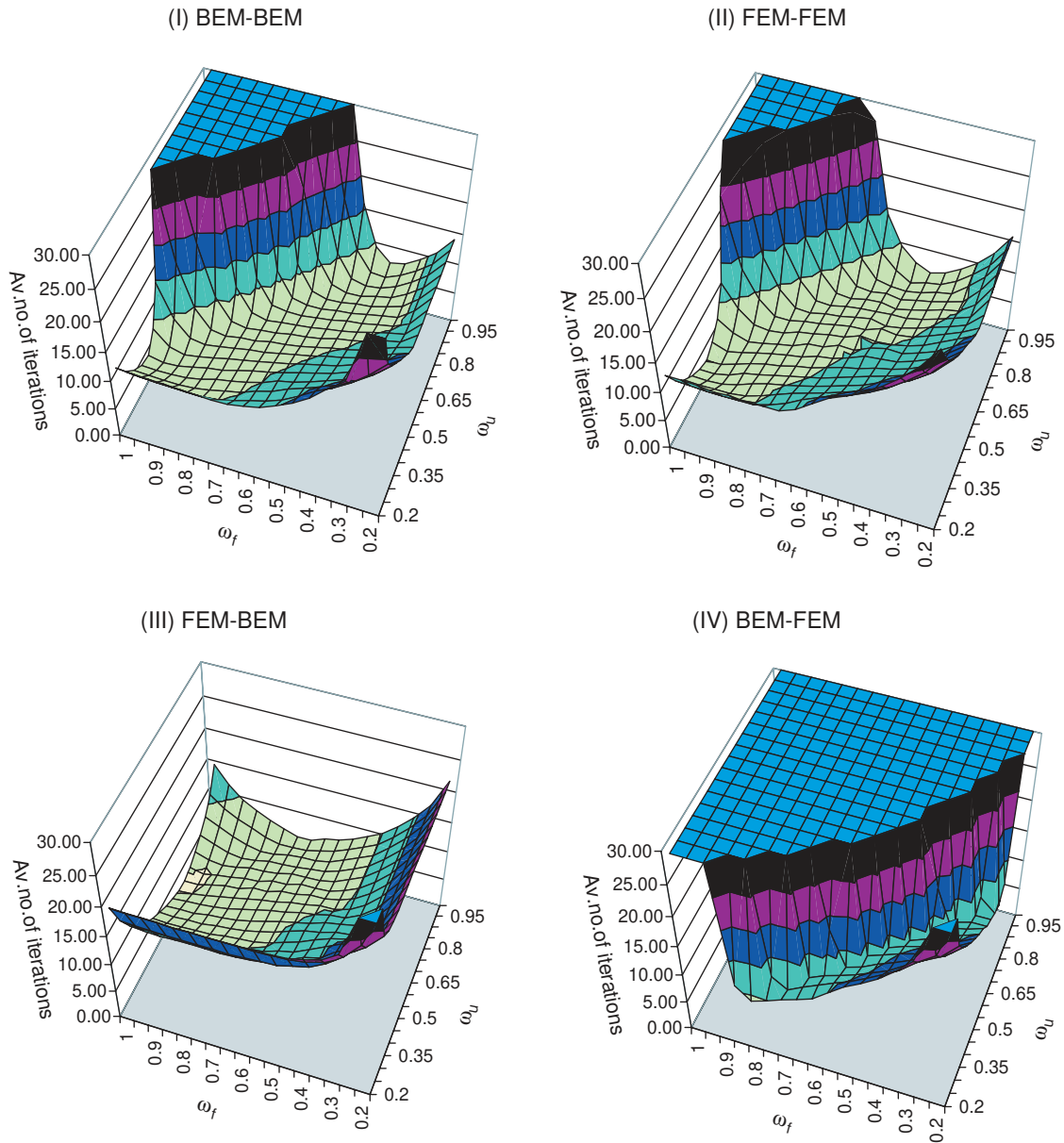


Fig. 3. Results of the parametric study for Models (I)–(IV) with $\Delta t_{FE}/\Delta t_{BE} = 1.0$: average no. of iterations per time step in dependency of the relaxation parameters ω_u and ω_f .

cases the parameters may be chosen identical, or one of them may be dropped at all.

From Fig. 3, it can be seen that the range from which the relaxation parameters can be chosen is very large for FEM–BEM coupling, while it is considerably smaller for FEM–FEM and BEM–BEM coupling. In the case of BEM–FEM coupling, it proves to be very difficult to achieve convergence at all. Optimal combinations of ω_u and ω_f exist in all cases; however, the optimum is found at different locations.

In order to address the effect of the time step ratio on the solution convergence, Model (III) is investigated for different time steps lengths of the FEM subdomain. From Fig. 4, it is observed that for very small FEM time step durations (as compared to the BEM time step durations), the convergence

behaviour becomes even more favourable. Whereas, if the time step ratio is 0.7 or 1.5, convergence cannot be ensured for combinations, where both relaxation parameters are close to one.

To conclude, it is very difficult to obtain general guidelines for the choice of the relaxation parameters. One recommendation seems to be obvious for cases, where an FEM and a BEM subdomain are involved: always take the FEM subdomain as Ω_1 in the proposed algorithm. Moreover, if in such cases the time step durations can be chosen equally, or with a small ratio $\Delta t_{FE}/\Delta t_{BE}$, both relaxation parameters should be chosen close to one. The combination $\omega_u = 1.0$ and $\omega_f = 0.75$ seems to be a good choice in the majority of those cases.

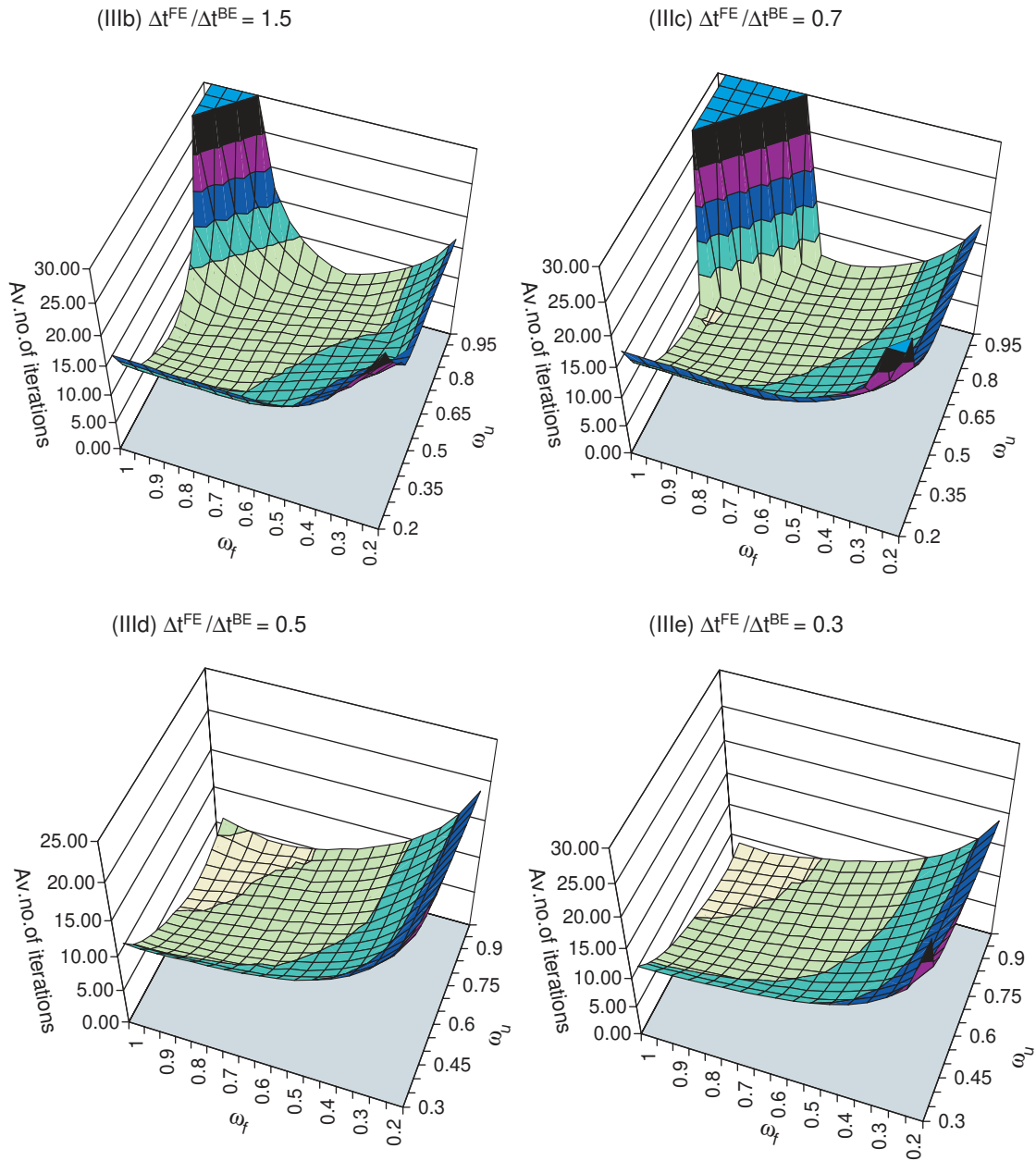


Fig. 4. Results of the parametric study for the FEM–BEM models (IIIb)–(IIIe), using different time step ratios $\Delta t_{\text{FE}}/\Delta t_{\text{BE}} = 1.5, 0.7, 0.5, 0.3$: average no. of iterations per time step in dependency of the relaxation parameters ω_u and ω_f .

Finally, it should be mentioned that the employment of a second relaxation substep (‘double relaxation’) seems to be of no significant advantage in the linear calculations analysed here. The second substep may be dropped without deteriorating the characteristics of the algorithm. However, if non-linear material behaviour is taken into account in one or more of the subdomains, the double relaxation clearly improves the convergence characteristics of the algorithm. This is shown by some non-linear calculations which were performed by the authors. Systematic studies on this point are being done at present.

Moreover, further studies, considering the stiffness ratios and other factors, should be undertaken for the proposed algorithm, as it was done previously, e.g. for several

FEM–BEM iterative coupling algorithms applied to stationary problems in Ref. [31].

6. Numerical examples

6.1. D-wave propagation

By means of an illustrative example, the validity of the results obtained from the proposed method is shown. The results are compared to analytical solutions as well as to solutions obtained by a direct coupling approach.

The employed model is very similar to that from the parametric studies given in Section 5, but with slightly different

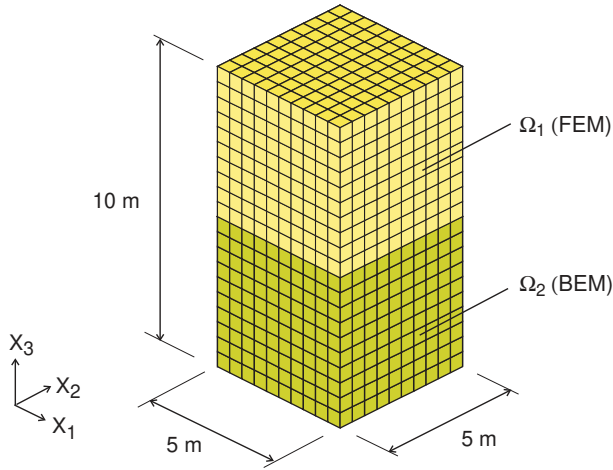


Fig. 5. FEM–BEM discretization of the elastic rod employed for the 1D wave propagation example.

dimensions and material parameters. The discretization is chosen much finer, employing elements with linear shape functions and with an edge length of 0.5 m constantly (Fig. 5). For this example, only an FEM–BEM model is considered, where the FEM subdomain is the upper, loaded part of the rod. Thus, the discretization consists of 1000 finite elements and 600 boundary elements.

The material parameters, corresponding to a linearly elastic material, are: Young’s modulus $E=2.66 \times 10^5 \text{ kN/m}^2$, Poisson’s ratio $\nu=0.33$, and mass density $\rho=2.0 \text{ t/m}^3$ (P-wave velocity $c_1=443.9 \text{ m/s}$).

The boundary conditions are chosen in a way that the results allow a comparison with a 1D problem, for which an analytical solution exists [38]. The rod is subjected to a Heaviside forcing function $p(t)=4.0 \text{ kN/m}^2 H(t)$ at the top surface, while at all other surfaces, the normal displacements are restraint to zero.

The time step duration for the BEM subdomain is $\Delta t_{BE}=0.00125 \text{ s}$ ($\beta=1.11$). Two different time steps for the FEM subdomain are selected, namely $\Delta t_{FE}=1.0 \Delta t_{BE}$ and $0.5 \Delta t_{BE}$. Furthermore, for one calculation, some numerical damping is introduced by selecting values for the Newmark time

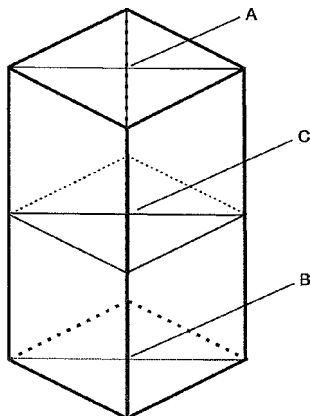


Fig. 6. Locations of the evaluation points A–C in the elastic rod model.

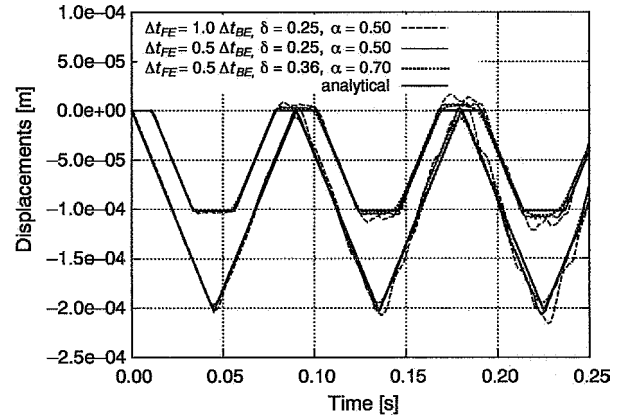


Fig. 7. Vertical displacements at points A and C, considering different time step relations and Newmark parameters.

integration parameters [1] which slightly deviate from the trapezoidal rule: $\delta=0.36$ and $\alpha=0.70$.

The convergence parameters are chosen as $\omega_u=1.0$ and $\omega_f=0.75$, corresponding to the optimal range of these parameters found from the parametric study. The average number of iterations per time step was 3.7, 3.4 and 2.9, respectively, in the three calculations.

The response of the rod is investigated at three points (Fig. 6), namely at point A at the center of the loaded (top) surface, at point B at the center of the bottom surface, and at point C at the center of the coupling interface. The respective results are shown in Figs. 7–9, where they are compared to the analytical solution (thick solid line).

The case with $\Delta t_{FE}=1.0 \Delta t_{BE}$ was also analysed by a direct coupling approach [40]. The results were found to be identical to those obtained by the proposed iterative coupling algorithm, and are therefore not explicitly shown here. The computer times, however, were considerably different: 14,000 CPU seconds for the iterative coupling as opposed to 25,500 CPU seconds for the direct coupling, measured on a normal PC with a 1000 MHz Pentium IV processor. In these timings, computation of the BEM influence matrices is not included.

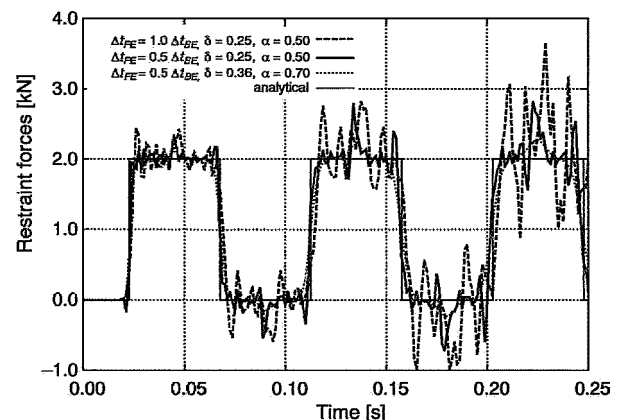


Fig. 8. Vertical restraint forces at point B (bottom of the rod), considering different time step relations and Newmark parameters.

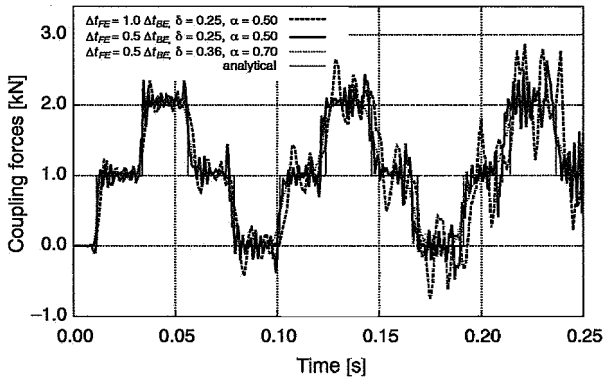


Fig. 9. Vertical coupling forces at the interface (point C), considering different time step relations and Newmark parameters.

In both cases, LU decomposition is employed for the solution of the equation systems, where the system matrix or matrices are decomposed only once for all time steps (since they are constant).

From the curves it can be observed that the displacement results obtained with the new coupling approach do match the analytical solution very well (Fig. 7), while the traction results exhibit some non-physical oscillations, when the trapezoidal rule is applied for the time integration (Figs. 8 and 9). These oscillations can be considerably reduced by choosing larger values of the Newmark parameters. Furthermore, it can be observed that the use of different time step durations in the subdomains is very important, since FEM analyses usually do not give proper results for time step durations that are best suited for BEM analyses. Using a smaller time step duration for the FEM subdomain than for the BEM one yields results that are much closer to the analytical solution than in the case of identical time step durations for both subdomains.

6.2.. Slender wall excited by incident wave

The next example deals with a more realistic earthquake-engineering example, namely a slender wall, which is excited by an incident displacement wave. The considered system is shown in Fig. 10. The soil (i.e. a reasonable part of the traction-free surface of the halfspace) is discretized with 132 boundary elements, while the wall is represented by 32 finite elements. All elements have edge lengths of 2.0 m and are based on

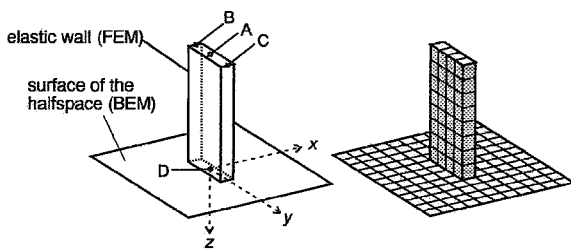


Fig. 10. Wall–soil system under consideration: discretization (right) and locations of the evaluation points A–D (left). All element edge lengths are 2.0 m.

Table 2
Material parameters used in the model

	Wall	Soil
Mass density (ρ (t/m ³))	1.8	1.8
Young’s modulus, E (kN/m ²)	1.0×10^7	5.0×10^7
Poisson’s ratio ν (-)	0.25	0.4
P-wave velocity, c_1 (m/s)	2582.0	771.5
S-wave velocity, c_2 (m/s)	1490.7	314.9

quadratic shape functions in space. The material parameters are given in Table 2.

The input motion is applied as an incident plane wave field, where the time variation is given by a Ricker wavelet [23] with a dominant period of $T_0=0.0536$ s, corresponding to the second mode of vibration of the wall when considered as a rigidly supported cantilever beam, and an amplitude of $a=0.02$ m. The time shape of the Ricker wavelet is shown in Fig. 11. The wave propagation direction is given by the vector $p=(0, 1, -1)^T$, while the direction of particle displacements (polarization) is $d=(1, 0, 0)^T$, such that the wall is excited in its ‘weak direction’ (x).

The convergence parameters $\omega_u=1.0$ and $\omega_f=0.75$ are used, and the time step duration for the BEM subdomain is $\Delta t_{BE}=0.0013$ s ($\beta=1.0$). Three analyses are performed, employing different time steps for the FEM subdomain, namely $\Delta t_{FE}=1.0 \Delta t_{BE}$, $0.5 \Delta t_{BE}$ and $0.25 \Delta t_{BE}$.

The displacement responses of the system are evaluated at four distinct points of the wall (see Fig. 10, left): point A is located at the center of the top surface of the wall, Points B and C can be found at its upper edges, and Point D is assumed at the center of the bottom cross-section, i.e. at the soil–structure interface. The time histories of the displacements at these four points are given in Figs. 12 and 13. It can be seen that resonance oscillations are excited, with the observed period being different from the dominant period of the incident wave. Some higher modes are excited in the longitudinal (y) direction of the wall, as can be seen from comparison of the responses at the three points at the top of the wall. This is due to the fact that the incident SH wave does not reach the wall over its whole length at the same time, but rather propagates along the footing of the wall. Since, the wave propagation speed inside the wall is significantly higher than in the soil, superposition of refracted and reflected waves generates a complicated pattern within the wall, exciting a 2D oscillation mode. It is interesting to note that at the edges much higher amplitudes are observed than at the center.

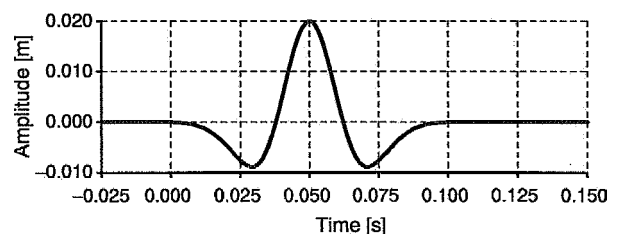


Fig. 11. Time shape of the incident wave (Ricker wavelet).

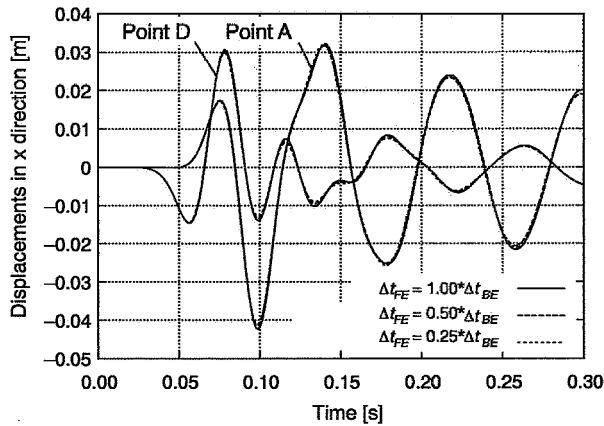


Fig. 12. Response of the slender wall due to the incident wave: time histories of the displacements in x -direction at points A (top of the wall) and D (wall–soil interface).

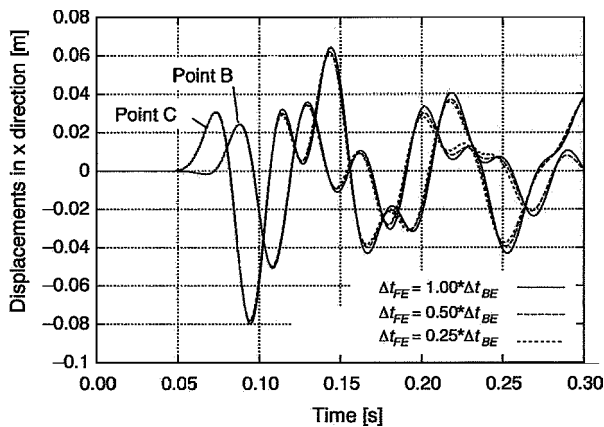


Fig. 13. Response of the slender wall due to the incident wave: time histories of the displacements in x -direction at points B and C at the top of the wall.

Comparing the results obtained with different FE time step durations, once more some differences in the calculated responses are observed. The smaller the FE time step size, the smaller the amplitudes of vibration. This corresponds to the observations from the elastic rod example (Section 6.1), where the displacement amplitudes are over-estimated, when large FE time step durations are used (Fig. 7).

7. Conclusion

An iterative coupling algorithm for FEM and BEM subdomains in 3D, transient elastodynamic analyses has been presented, which may be categorized as the sequential Neumann–Dirichlet method with double relaxation.

The major advantage of this approach, as compared to conventional, direct coupling procedures, can be seen in the fact that the subdomain system equations are solved separately, using solution algorithms which are optimized with respect to the employed subdomain methods. Consequently, the systems of equations to be solved are much smaller than the conventional coupled systems. In addition, the iterative

coupling offers two advantages: it is straightforward to use different time steps in each subdomain, and, moreover, to take into account non-linearities (in the FEM subdomain) in the same iteration loop that is needed for the coupling.

By means of a parametric study, the convergence characteristics of the proposed algorithm were investigated. It was found that the convergence behaviour is considerably influenced by the employed combination of subdomain analysis methods (FEM and/or BEM), and by the selection of the respective time step durations. Moreover, the convergence behaviour strongly depends on the choice of the two relaxation parameters which are contained in the algorithm. In the linear calculations analysed in this paper, however, the second relaxation substep is of no significant advantage. Whereas, some further calculations indicate that clear advantages exist, if non-linearities are taken into account.

The validity of the proposed method has been shown by means of two numerical examples. First, a 3D, finite rod was analysed, simulating a 1D wave propagation problem. The results were compared to the analytical solution as well as to results obtained by the conventional direct coupling method, and it was seen that the proposed algorithm yields excellent accuracy. Second, the response of a slender wall to an incident ‘seismic’ wave field was analysed, illustrating the applicability of the algorithm to more sophisticated, 3D problems.

Acknowledgements

The authors would like to thank the *Deutsche Forschungsgemeinschaft* (DFG) for the financial support of their studies through a scholarship, granted to the second author, within the graduate research program (*Graduiertenkolleg*) ‘Ocean Engineering Structures’.

References

- [1] Bathe K-J. Finite element procedures. Englewood Cliffs, NJ: Prentice Hall; 1996.
- [2] Zienkiewicz OC, Taylor RL. The finite element method. 5th ed. Butterworth-Heinemann: Oxford; 2000.
- [3] Kane JH. Boundary element analysis in engineering continuum mechanics. Englewood Cliffs, NJ: Prentice-Hall; 1994.
- [4] Bonnet M. Boundary integral equation methods for solids and fluids. Chichester: Wiley; 1995.
- [5] Domínguez J. Boundary elements in dynamics. Southampton: Computational Mechanics Publications; 1993.
- [6] Zienkiewicz OC, Kelly DM, Bettes P. The coupling of the finite element method and boundary solution procedures. *Int J Numer Methods Eng* 1977;11:355–76.
- [7] Spyarakos C, Beskos DE. Dynamic response of flexible strip foundations by boundary and finite elements. *Soil Dyn Earthq Eng* 1986;5(2): 84–96.
- [8] von Estorff O. Coupling of BEM and FEM in the time domain: some remarks on its applicability and efficiency. *Comput Struct* 1992;44(1/2): 325–37.
- [9] Beskos DE, Krauthammer T, Vardoulakis I, editors. Dynamic soil–structure interaction. Proceedings of the international symposium on dynamic soil–structure interaction, Minneapolis, 4–5 September. Rotterdam: A.A. Balkema; 1984.

- [10] von Estorff O. Zur Berechnung der dynamischen Wechselwirkung zwischen Bauwerken und ihrer Umgebung mittels zeitabhängiger Randintegralgleichungen. Mitteilung: Institut für Konstruktiven Ingenieurbau der Ruhr-Universität Bochum; 1986.
- [11] Karabalis DL, Beskos DE. Dynamic soil–structure interaction. In: Beskos [41], p. 499–562 [Chapter 11].
- [12] Brebbia CA, Telles JCF. Fluid–structure interaction. In: Beskos [41], p. 563–87 [Chapter 12].
- [13] Beer G. Programming the boundary element method. Chichester: Wiley; 2001.
- [14] Trevelyan J. Boundary elements for engineers—theory and applications. Southampton: Computational Mechanics Publications; 1994.
- [15] Araújo FC, Alberto DR, Dora C. Analysis of 3D time-dependent acoustic problems via a generic BE substructuring algorithm based on iterative solvers. *Eng Anal Bound Elem* 2003;27:705–16.
- [16] Beskos DE. Boundary element methods in dynamic analysis. *Appl Mech Rev* 1987;40(1):1–23.
- [17] Beskos DE. Boundary element methods in dynamic analysis. Part II (1986–1996). *Appl Mech Rev* 1997;50(3):149–97.
- [18] Beskos DE. Dynamic analysis of structures and structural systems. In: Beskos DE, Maier G, editors. *Boundary element advances in solid mechanics*, no. 440 in CISM courses and lectures. Wien: Springer; 2003. p. 1–53 [Chapter 1].
- [19] Karabalis DL, Beskos DE. Dynamic response of 3D flexible foundations by time domain BEM and FEM. *Soil Dyn Earthq Eng* 1985;4:91–101.
- [20] Fukui T. Time marching BE–FE method in 2D elastodynamic problems. In: *Proceedings of the international conference on boundary element methods IX*, Stuttgart.
- [21] von Estorff O, Prabucki MJ. Dynamic response in the time domain by coupled boundary and finite elements. *Comput Mech* 1990;6:35–46.
- [22] Pavlatos GD, Beskos DE. Dynamic elastoplastic analysis by BEM/FEM. *Eng Anal Bound Elem* 1994;14:51–63.
- [23] Adam M. Nonlinear seismic analysis of irregular sites and under ground structures by coupling BEM to FEM. PhD Thesis. Graduate School of Natural Science and Technology, Okayama University; March 1997.
- [24] Abouseeda H, Dakoulas P. Nonlinear dynamic earth dam–foundation interaction using a BE–FE method. *J Struct Dyn Earthq Eng* 1998;27(12): 917–36.
- [25] Yazdchi M, Khalili N, Valliappan S. Non-linear seismic behaviour of concrete gravity dams using coupled finite element–boundary element technique. *Int J Numer Methods Eng* 1999;44:101–30.
- [26] Firuziaan M, von Estorff O. Transient 3D soil/structure interaction analyses including nonlinear effects. In: Grundmann H, Schuëller GI, editors. *Structural dynamics—EURODYN2002*, vol. 2. Lisse: Swets and Zeitlinger; 2002. p. 1291–6.
- [27] Park KC, Felippa CA. Partitioned analysis of coupled systems. In: Belytschko T, Hughes TJ, editors. *Computational methods for transient analysis*. Amsterdam: North-Holland; 1983. p. 157–219 [Chapter 3].
- [28] Rizos DC, Wang Z. BEM–FEM solutions for direct time domain soil–structure interaction analysis. *Eng Anal Bound Elem* 2002;26:877–88.
- [29] Mok DP. Partitionierte Lösungsansätze in der Strukturmechanik und der Fluid-Struktur-Interaktion. Bericht Nr. 36: Institut für Baustatik der Universität Stuttgart; 2001.
- [30] Soares Jr D, von Estorff O, Mansur WJ. Iterative coupling of BEM and FEM for nonlinear dynamic analyses. *Comput Mech* 2004;34:67–73.
- [31] El-Gebeily M, Elleithy WM, Al-Gahtani HJ. Convergence of the domain decomposition finite element–boundary element coupling methods. *Comput Methods Appl Mech Eng* 2002;191(43):4851–68.
- [32] Elleithy WM, Tanaka M. Interface relaxation algorithms for BEM–BEM coupling and FEM–BEM coupling. *Comput Methods Appl Mech Eng* 2003;192:2977–92.
- [33] Lin C-C, Lawton EC, Caliendo JA, Anderson LR. An iterative finite element–boundary element algorithm. *Comput Struct* 1996;39(5): 899–909.
- [34] Feng YT, Owen DRJ. Iterative solution of coupled FE/BE discretization for plate–foundation interaction problems. *Int J Numer Methods Eng* 1996;39(11):1889–901.
- [35] Elleithy WM, Al-Gahtani HJ, El-Gebeily M. Iterative coupling of BE and FE methods in elastostatics. *Eng Anal Bound Elem* 2001;25:685–95.
- [36] Manolia GD, Beskos DE. *Boundary element methods in elastodynamics*. London: Unwin Hyman; 1988.
- [37] Neidhart T. Lösung dreidimensionaler linearer Probleme der Bodendynamik mit der Randelementmethode. Veröffentlichungen Nr. 131, Karlsruhe: Institut für Bodenmechanik und Felsmechanik der Universität Fridericiana; 1994.
- [38] Schanz M. Wave propagation in viscoelastic and poroelastic continua—a boundary element approach. *Lecture notes in applied mechanics*, vol. 2. Berlin: Springer; 2001.
- [39] Elleithy WM, Tanaka M. Domain decomposition coupling of FEM and BEM. *Transactions of JSCES paper no. 20010050*.
- [40] von Estorff O, Hagen C. Dynamic response of blocks on a halfspace including nonlinear effects. *Strojnícky Časopis—J Mech Eng* 2003;54(5–6):277–92.